Journal of Materials Chemistry C

Accepted Manuscript

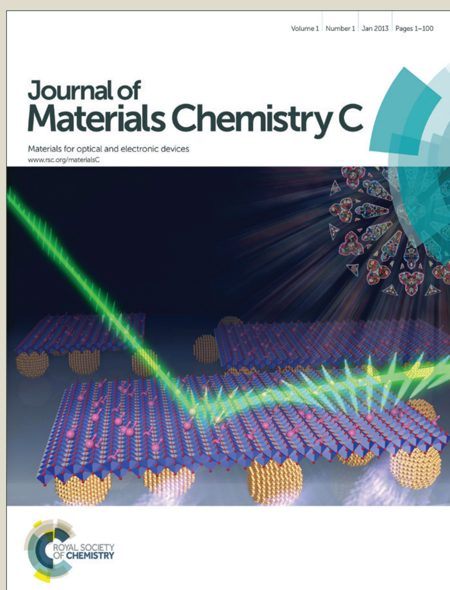

This is an *Accepted Manuscript*, which has been through the Royal Society of Chemistry peer review process and has been accepted for publication.

Accepted Manuscripts are published online shortly after acceptance, before technical editing, formatting and proof reading. Using this free service, authors can make their results available to the community, in citable form, before we publish the edited article. We will replace this *Accepted Manuscript* with the edited and formatted *Advance Article* as soon as it is available.

You can find more information about *Accepted Manuscripts* in the Information for Authors.

Please note that technical editing may introduce minor changes to the text and/or graphics, which may alter content. The journal's standard Terms & Conditions and the Ethical guidelines still apply. In no event shall the Royal Society of Chemistry be held responsible for any errors or omissions in this *Accepted Manuscript* or any consequences arising from the use of any information it contains.

ROYAL SOCIETY OF CHEMISTRY

www.rsc.org/materialsC

Effects of O_3 and H_2O as Oxygen Sources in Atomic Layer Deposition of HfO_2 Gate Dielectrics at Different Deposition Temperatures

Sang Young Lee, Hyo Kyeom Kim, Jong Ho Lee, Il-Hyuk Yu, Jae-Ho Lee, and Cheol Seong Hwang*

Department of Materials Science and Engineering and Inter-university Semiconductor Research Center, Seoul National University, Seoul 151-744, Korea

Abstract

Variations in the growth behavior, physical and electrical properties, and microstructure of the atomic layer deposited (ALD) HfO_2 gate dielectrics were examined with two types of oxygen sources: O_3 and H_2O for the given Hf-precursor of $Hf[N(CH_3)(C_2H_5)]_4$. The ALD temperature windows for the O_3 and H_2O were 160-320°C and 160-280°C, respectively, with the growth rate of HfO_2 using O_3 being higher than that of the films using H_2O within the ALD window. While the film density of HfO_2 using O_3 decreased, that of HfO_2 using H_2O increased with the decreasing ALD temperature. As the deposition temperature decreased, the amount of impurity in the HfO_2 film with the O_3 oxidant increased due to the insufficient reaction, which led to the crystallization of the HfO_2 film into the tetragonal structure after the post-deposition annealing at 600°C. The films with a lower density and a higher carbon-impurity concentration retained the portion of the tetragonal phase (~30%) to the highest annealing temperature of 1000°C. However, the HfO_2 films grown at 200°C with H_2O showed the best electrical performance, which could be ascribed to the highest density, low impurity concentration, and negligible involvement of the interfacial low dielectric layer.

*Corresponding author: cheolsh@snu.ac.kr

Journal of Materials Chemistry C Accepted Manuscript

I. Introduction

HfO_2 thin films have been widely used in the semiconductor industry, especially in the mass production of Si-based metal insulator semiconductor field effect transistors (MISFETs), as high dielectric constant (high-k) gate dielectric thin films since 2007 [1-3]. Atomic layer deposition (ALD) has many advantages in the formation of gate dielectric thin films for extremely scaled planar or three-dimensional structured devices due to its self-limiting growth behavior, which confirms a low leakage current, high dielectric constant, and atomic-level precise thickness control. However, more studies are required to fabricate Hf-based dielectric films with even higher-k values ($k > 30$) for further scaled MISFETs that require an equivalent oxide thickness (EOT) < ~0.5 nm. In addition, there is a greater challenge to apply ALD-processed HfO_2 to high-mobility channel materials such as III-V or II-V compound semiconductors for the n-type MISFET and Ge for the p-type MISFET [2-3]. These challenges are known to be caused by the unstable interfaces between the HfO_2 film and the high-mobility substrates [4-8], the status of which is largely influenced by the detailed ALD conditions. Several other high-k dielectrics, such as Al_2O_3, La_2O_3, and $LaLuO_3$ [9-12], have been adopted for the high-mobility substrates, but it might be best if the use of HfO_2 can be extended to these substrates considering its mature process equipment, conditions, and contamination-control protocols in mass-production lines.

Because of these important aspects of HfO_2 in advanced semiconductor chips, ALD of the HfO_2 film is one of the most extensively studied ALD processes. While the commercialized ALD process of the HfO_2 film for high-k gate dielectric application adopted $HfCl_4$ and H_2O as the Hf-precursor and the oxygen source, respectively [13-16], alternative ALD processes that utilize metal-organic Hf-precursors and O_3 are still under intensive research [17-19]. The major driving force for the search for such an alternative ALD process is the difficulty in handling the powdery $HfCl_4$ precursor, which requires a high vaporization temperature (~200^oC) to achieve sufficient vapor pressure, and hardware problems related to the corrosive reaction by-product (HCl) of the process [20]. The ALD process of the HfO_2 film using $HfCl_4$ and H_2O could be performed well at the substrate temperatures (T_s) of 300 - 400^oC without the concern related to the thermal decomposition of the $HfCl_4$. In contrast, most

Journal of Materials Chemistry C Accepted Manuscript

metal-organic Hf-precursors suffer from such degradation at a relatively low T_s; most Hf-alkoxides and Hf-alkylamides thermally decomposed at temperatures lower than ~200-250 and 300-350°C, respectively, the accurate values of which are dependent on the detailed process conditions [21-23]. (Modified) cycloropentadienyl (Cp)-based Hf-precursors have shown higher thermal decomposition temperatures (of up to ~ 400°C) [24], but ALD using the Cp-based Hf-precursors usually has a lower growth rate (< ~0.05 nm/cycle) than other metal-organic Hf-precursors, presumably due to the higher bulkiness of the ligand and its superior thermal stability [24-25].

O_3 is attracting increasing interest as the oxygen source for the ALD of various oxide films due to its generally higher oxidation potential than H_2O at a normal ALD temperature range. The higher oxidation power of O_3 is particularly attractive when the ALD process temperature approaches the upper limit of the ALD temperature window, where the (partial) thermal decomposition of Hf-precursors results in C-impurity contamination in the film. H_2O can hardly remove the cracked C from the ligands, but the strong oxidation power of O_3 can remove it by forming volatile CO and CO_2 [17]. O_3 has been highly accepted in capacitor dielectric layer formation for dynamic random access memory (DRAM), such as ZrO_2 and Al_2O_3, where the as-high-as-possible ALD temperature was preferred to achieve higher crystallinity accompanied by a higher dielectric constant. However, for the MISFET application, O_3 almost always induces interfacial thin SiO_2 formation during the ALD of the HfO_2 film, which really deteriorated the overall k-value of the gate dielectric layer when the high-k HfO_2 film was within the practical thickness range (2-4 nm) [26]. Therefore, there must be an appropriate compromise between the attainable lowest EOT and the film quality by controlling the T_s, O_3 concentration and the O_3 pulse time [27]. The lower T_s generally induces a lower interfacial layer (IL, mostly SiO_2 or Hf-silicate), but the high quality of the high-k film must be sacrificed under such condition. Recently, a technology where adoption of a chemically active metal gate, which is active enough to scavenge the oxygen from the IL without degrading the quality of HfO_2, was developed [28]. This means that the IL can be removed by the post-process after the gate formation [29-30]. Such removal of IL was inevitably accompanied by the degradation of the carrier mobility and reliability in the MISFET device, but such deterioration of the device performance could be overcompensated for

Journal of Materials Chemistry C Accepted Manuscript

by the increased capacitance effect [28,30]. Therefore, the adoption of O_3 for MISFET fabrication has a higher probability in the most recent integration flow. Another advantage of O_3 over H_2O is its faster purge-out speed, especially when the ALD temperature is lower than < ~150°C, during which the purge-out speed of H_2O becomes very slow [17,31]. In contrast, the chemical activity of O_3 at such a low temperature drops quickly, so adoption of O_3 for low-temperature ALD is not desirable. In this regard, the maintained high chemical activity of H_2O toward the ligand-exchange reaction of ALD oxide films could be highlighted.

Another important task of the ALD of high-k films is the phase control to achieve an even higher k value, which has been less focused on the MISFET field compared with the capacitor dielectric for DRAM. The k-value of HfO_2 is largely dependent on its crystallographic phases (amorphous and monoclinic, ~15, and tetragonal and cubic, ~30) [32-33], which must be largely determined by the detailed deposition as well as the post-deposition annealing (PDA) conditions. Although the thermodynamic stable phase of HfO_2 at the ALD temperature (160-360°C in this study) and at the typical PDA temperature (T_{PDA}, up to 1000°C) is monoclinic [34], there have been many reports on the formation of tetragonal- or cubic-phase HfO_2 thin films by controlling the microstructure of the films [35-39]. In this report, the higher-k HfO_2 phase is considered the tetragonal phase because it is usually difficult to clearly distinguish the tetragonal phase from the cubic phase in a thin HfO_2 film via laboratory X-ray diffraction. In addition, the k values of the two phases do not differ much and are also dependent on the crystallographic directions [40]. Therefore, the higher-k phase could be tetragonal, cubic, or even a mixture of them, but a clear distinction was not attempted for as long as the phase was distinguished from the monoclinic phase. Although there are diverse detailed methods of such transformation of HfO_2 to the higher-k phases [39,41], they basically rely on the grain size effect (a smaller grain size is preferred in the higher-k phase) because the surface (or the grain boundary) energy of the higher-k phase is lower than that of the monoclinic phase [42-44]. Therefore, varying the T_s and the types of oxygen sources could be a viable way to vary the grain size at the as-deposited state or after the PDA, and to achieve the higher-k phase.

For the III-V and Ge substrates, the different oxidation powers of H_2O and O_3 at different T_s values

Journal of Materials Chemistry C Accepted Manuscript

may provide a certain ALD process window for the HfO_2 films, where the adverse interfacial effects are minimized. Additionally, the application of the very-low-temperature ALD of high-k dielectric films to transparent and flexible electronic devices is being actively studied. Some of the authors recently reported the growth behavior and film properties of the HfO_2 film at a T_s as low as 30°C using a high O_3 concentration (350 g/m^3) as the oxygen source in ALD [31]. Therefore, in this study, various properties of ALD-HfO_2 films using tetrakis-ethylmethylamino-hafnium {$Hf[N(CH_3)(C_2H_5)]_4$, TEMAHf} as the Hf-precursor and different oxygen sources (H_2O and O_3) grown at different T_s values are examined systematically. While the mentioned previous reports focused on extending the higher end of the ALD temperature window to higher T_s values [17,21-25], this study attempted to explore the possible deposition of high-quality ALD HfO_2 films at lower T_s values, which could provide an essential clue to the achievement of promising growth and electrical behavior of HfO_2 on high-mobility substrates for futuristic MISFET or on plastic substrates for flexible-device fabrication, although this study dealt with only Si substrates. The evolution of phases according to detailed ALD and PDA conditions is also studied in detail.

II. Experiment Procedure

The HfO_2 films were deposited on deionized-water-diluted, hydrofluoric (HF)-acid-cleaned p-type Si(100) wafers with 10Ωcm resistivity via ALD at substrate temperatures (T_s) of 160-360°C, using TEMAHf as the Hf-precursor and different oxygen sources (H_2O and O_3). O_3 was generated by flowing a mixture of O_2 (1,350 sccm) and N_2 (10 sccm) into an ozone generator (Astex, AX8200). The ozone concentration was fixed at 170 g/m^3. The optimized condition of the Hf-precursor pulse-Ar purge-H_2O (or O_3) pulse-Ar purge time was 3-20-3-10 s, respectively, where an Ar purge gas flow rate of 200 standard cubic centimetres per min (sccm) was adopted. The Hf-precursor vapor was achieved by heating the Hf-precursor canister to 60°C and transporting it into the cross-flow-type ALD reactor, which is capable of processing an 8-inch-diameter wafer, with the help of Ar carrier gas with a flow rate of 200 sccm. The deionized water with which a steel canister was filled was cooled down to 5°C to achieve the appropriate H_2O vapor pressure.

Journal of Materials Chemistry C Accepted Manuscript

The thickness of the HfO_2 film was measured with a single-wavelength ellipsometer (L116D, Gaertner Co.) and a spectroscopic ellipsometer (SE, ESM-300, Wollam Co.). The crystalline structure of the HfO_2 film was analyzed via glancing angle incidence X-ray diffraction (GAXRD, X'Pert PRO MPD, PANalytical Co., X-ray incidence angle 2°). The surface morphology was examined with a scanning electron microscope (SEM, S-4700, Hitachi) and an atomic force microscope (AFM, JSPM-5200, JEOL Co.). The root-mean-squared (RMS) roughness of the thin films was measured with the same AFM. The density and roughness of the thin films were measured via X-ray reflection (XRR, using the same equipment as in the XRD). The microstructure of the films was observed via cross-sectional high-resolution transmission electron microscopy (HRTEM, JEM 3000F, JEOL). The HRTEM sample was prepared via standard sample bonding, grinding, and ion milling. The chemical bonding states of the HfO_2 films were examined with the X-ray photoelectron spectra (XPS, Sigma Probe, ThermoVG) using a monochromatic Al Kα source (1486.6 eV) to excite the photoelectrons. The positions of all the peaks were calibrated for the C 1s peak of the adventitious carbon-carbon binding energy to be assigned at 284.5 eV. The carbon impurity concentration was confirmed via Auger electron spectroscopy (AES, Perkin-Elmer 660) in the depth profiling mode, which is performed via Ar^+ ion sputtering.

To examine the electrical property, metal-insulator-semiconductor (MIS) capacitors were fabricated with sputter-deposited Pt top electrodes through a shadow mask with 300 □m-diameter holes. Forming gas annealing was performed to passivate the dangling bonds at the interface between the oxide and the substrate under a H_2 (5%)/N_2 (95%) mixture gas atmosphere at 450°C for 10 min. The capacitance-voltage (C-V) was measured using an HP 4194A impedance analyzer at the frequency of 100 kHz. The oxide leakage current (J_g) was investigated using an HP 4140B picoammeter/DC voltage source. The Pt gate was biased while the Si substrate was grounded during the electrical measurements. The capacitance equivalent thickness (CET) was estimated from the accumulation capacitance values when the films were thick enough (> ~10 nm), and from the fitting of the C-V curves to the theory using the CVC program [45].

Journal of Materials Chemistry C Accepted Manuscript

III. Results and Discussion

First, the changes in the film growth rate (the thickness increase per ALD cycle) and the film density were examined as functions of T_s. Figures 1 (a) and (b) show the variations in the growth rate and the film density of the HfO_2 film, respectively, as functions of T_s. Here, the growth rate was estimated from the slope of the best-linear-fitted graphs of the data points that showed the film thickness as a function of the ALD cycles for each condition (data not shown). Therefore, the data presented in Figure 1 (a) are free from the possible influence of any interfacial layer (IL) growth. In the case of the HfO_2 with O_3, the film growth rate monotonically decreased with the increasing T_s up to ~320°C, but suddenly increased at the T_s of 360°C. This suggests that the ALD window could be assigned to the T_s of ~240 to 320°C, where the variation in the growth rate is minimized, and the growth rate was ~0.1 nm/cycle, which is similar to that in previous reports [16-17]. The sudden increase in the growth rate at the T_s of 360°C revealed that the film growth was by then governed by the thermal cracking of the Hf-precursors on the O_3-pulsed surface. The increased growth rate at T_s < ~240°C could be ascribed to the decreased film density and the increased impurity concentration in the films, which will be shown later.

In the case of HfO_2 with H_2O, the film growth rate was generally lower than that with the O_3 within the ALD T_s window (< 280°C) which could be ascribed to the lower oxidizing power of H_2O than of O_3 [15]. Within the ALD temperature window, the ALD film growth rate is generally governed by the steric hindrance effect of the chemically adsorbing precursors. When the Hf-precursor was pulsed on the O- or OH^--terminated surfaces, for the O_3 and H_2O cases, respectively, a certain part of the ligands was removed by the ligand-exchange reaction. Depending on the chemical reactivity between the surface reaction sites (the O-radical or OH^--group) and the ligands of the Hf-precursor, the number of ligands left, and thus, the bulkiness of the chemisorbed species, is determined when this reaction is completed. The higher reactivity induced the lower bulkiness and the higher growth rate.

As the T_s exceeded 320°C, the growth rate increased abruptly, which again suggests that the thermal cracking of chemisorbed Hf-precursors is activated at this temperature and chemical vapor deposition (CVD)-like deposition occurs. It is interesting to note that the initiation temperature at which the

Journal of Materials Chemistry C Accepted Manuscript

CVD-like deposition reaction occurs is lower for H_2O even though its driving force toward the ALD-type deposition reaction in the lower T_s region appears to be lower than in the O_3 case. The accurate reasons for such disparate chemical activity of O_3 and H_2O toward CVD-type reaction at different T_s regions are not understood yet, but a hypothesis is given below.

Figure 1 (b) shows that the film density of HfO_2 was the highest (~8.5 g/cm^3) when HfO_2 was deposited with O_3 at a T_s of 280°C, but it is still substantially lower than the ideal value of bulk HfO_2 (9.68 g/cm^3). This highest value was similarly achieved at the T_s of 320°C, but it decreased significantly with the decreasing T_s down to 160°C. The film grown at a T_s of 360°C also showed a very low density, which could be ascribed to the CVD-like growth behavior of the film at such temperature. On the other hand, the layer-by-layer growth in the ALD mode at a lower T_s could induce films with a higher density despite the lower T_s. Even in the ALD mode, however, a too low T_s (< 200°C) provides the surface-adsorbed atoms with insufficient thermal energy for them to migrate and form a dense film. The insufficient thermal energy also induced an incomplete ligand exchange reaction, which resulted in the high impurity (carbon-related impurities) in the film, as will be shown later, and which also contributed to the lower film density.

In contrast, the film density of HfO_2 with H_2O increased monotonically with a decreasing T_s, and the highest density (~8.5 g/cm^3) was achieved at the lowest T_s of 160°C. While the low density of the films grown at the T_s of 320 and 360°C could be ascribed to the CVD-like growth behavior, as in the O_3 case, the decreasing density with the increasing T_s within the ALD window required different explanations from the usual temperature-dependent density of ALD films.

Figure 2 shows the AES depth profiling results of HfO_2 films grown at four different deposition conditions. The condition of 280°C O_3, as shown in Figure 2 (a), had the lowest carbon impurity contents (< 5 atomic %), which indicates that the ALD reaction fluently occurred under this condition. The HfO_2 film also contained Si with an approximate concentration of 5 atomic %, which must be diffused from the substrate. The Hf/O ratio was constant throughout the film thickness. The film grown at the same T_s with H_2O, as shown in Figure 2 (b), also had a low carbon impurity concentration, and the Hf/O ratio was also constant throughout the film thickness. In addition, the Si

Journal of Materials Chemistry C Accepted Manuscript

concentration was much lower than that in Figure 2 (a). This suggests that the Si diffusion observed in Figure 2 (a) was induced by the high oxidation potential of O_3 and not by the thermal energy of 280°C. O_3 could be well decomposed into O_2 and O-radicals at this T_s, and the resulting O-radicals induced the fluent ALD-type reactions to form the stoichiometric HfO_2. The high activity of the O-radicals adsorbed on the film surface induced the outward diffusion of Si from the substrate. In the case of the 200°C O_3, as shown in Figure 2 (c), a significant concentration of carbon impurity was observed, which was also seen in the previous report [36]. However, the Si concentration in the HfO_2 film was negligible in this case. It can also be seen that the Hf concentration was much lower than that in the film grown at a higher temperature and was non-uniform across the film thickness, but the oxygen concentration did not significantly differ. This suggests that some of the oxygen atoms might have combined with C (and also H, which cannot be detected by AES) and been contained in the film. This explains well the low film density in this case, as shown in Figure 1 (b). It appears that the

decomposition of O_3 into the O_2 and O-radicals at this T_s was not high enough, so the fluent ALD-type reaction did not occur. The almost negligible Si concentration in the films also supports this hypothesis, because the small difference in the T_s (80°C) was not expected to induce such a subtle difference in the thermal diffusion of Si into the HfO_2 film. The high carbon impurity concentration in the HfO_2 film was also reported under similar ALD conditions, except for the adoption of O_2 instead of O_3 at a T_s of 280°C by Cho et al. [39].

In contrast, the condition of 200°C H_2O, as shown in Figure 2 (d), resulted in lower carbon contents than in the film grown at 200°C with O_3, and the overall composition profiles did not significantly differ from that of the film grown at 280°C under the H_2O condition. These AES results suggest that the ALD behavior of the HfO_2 films with O_3 or H_2O is not simply governed by the oxidation power of the adopted oxygen source.

From these data, the deposition mechanisms of the HfO_2 film with O_3 or H_2O as the oxygen source could be as follows. The possible chemical reaction routes for the ALD of HfO_2 using TEMAHf and H_2O were carefully examined using molecular dynamic simulations based on the density functional theory [46]. In that study, it was concluded that the key ingredient that triggers the ALD reaction of the

Journal of Materials Chemistry C Accepted Manuscript

HfO_2 film to commence with the TEMAHf and H_2O was the supply of protons from the OH^- groups to the incoming TEMAHf molecules when they were pulsed on the OH^--terminated surface [28]. The donation of protons to the TEMAHf molecules and the chemical reaction with the TEMA ligands have a highly exothermic nature, which makes them occur fluently even at a very low temperature without involving the significant activation energy barrier. This is in quantitative agreement with the earlier suggestion on the two-step ALD mechanism based on the experiment results reported by Liu et al [17]. Therefore, it could be considered that the 160°C of T_s was high enough to induce the ideal ALD reaction between the TEMAHf-precursor and H_2O, and to produce HfO_2 films with a high density and a high growth rate. However, as the T_s increases, the surface concentration of the OH^- group decreases due to re-evaporation, which would inevitably induce sparse adsorption of TEMAHf-precursor molecules in the subsequent metal-precursor pulse step. Once the TEMAHf-precursor molecules sparsely adsorb on the growing surface, further ALD steps would produce a film with a porous structure because the subsequently impinging TEMAHf-precursor molecules must feel the steric hindrance effect when they attempt to fill in the empty surface sites that were formed in the previous ALD cycle. H_2O molecules may not feel such hindrance effect because they have much smaller molecular size. This could explain the tendency of growth and impurity concentration with respect to T_s, as shown in Figures 1 and 2, in the cases of ALD using H_2O. As the T_s exceeds 320°C, such proton diffusion may occur at a higher extent to form multiple layers composed of partially fragmented TEMAHf molecules in the Hf-precursor pulse step. This could significantly increase the growth rate, as shown in Figure 1 (a), but the multiple layers could have a less dense structure, which is in accordance with the results shown in Figure 1 (b). This is not correlated with the normal mechanism of film growth, wherein the increase in the deposition temperature promotes migration of an adatom and results in a high film density.

In contrast, in the case of ALD with O_3, a different mechanism should be invoked, because there is hardly any OH^- group [17] on the film surface, and therefore, there would be hardly any proton donation as well. Instead, in this case, when the Hf-precursor molecules were pulsed, they chemically adsorbed on the surface by temporarily making the coordination number metal centers of the

Journal of Materials Chemistry C Accepted Manuscript

TEMAHf molecules five from the reaction between them and the surface oxygen ions [46] that were contained in the previously grown HfO_2, or the O-radicals adsorbed at the Hf sites. When the O_3 was subsequently injected onto the O-TEMAHf-containing surface, it decomposed to the O_2 molecules and O-radicals, and the O-radicals reacted with the ethylmethylamide-ligands, which finally completed the ALD reaction. From the analysis of the reaction by-products of the TEMAH-O_3 ALD process, it was concluded that there was a low probability of replacing the ethylmethylamide-ligand with OH^- groups, but the Hf-N bond was replaced by the Hf-O bond, and the fragmented ethylmethylamide-ligands were decomposed into simpler compounds due to their combustion from their reaction with O_3 [17]. The decomposition of O_3 into the O_2 molecule and the O-radical must be thermally activated. Such reaction routes may involve a very high activation energy barrier that could thermally activate the overall reaction and lead to more effective ligand removal and a higher film density and purity at a higher T_s. O-radicals are not expected to diffuse to the chemically absorbing molecules in the precursor pulse step, as they are very different from the proton donation and diffusion in the case of ALD with H_2O, so the initiation temperature for the CVD-like behavior increased to 360°C, as shown in Figure 1 (a). Such a subtle difference in the reaction mechanism of ALD using H_2O and O_3 resulted in the following very distinctive film properties.

The evolution of crystalline phases according to the deposition and PDA conditions was examined using GAXRD. Figure 3 (a) shows the GAXRD spectra of the as-deposited films with an increasing film thickness when the films were grown at a T_s of 280°C using O_3. When the films were thinner than ~25 nm, they retained amorphous structure; but they started to be crystallized to the monoclinic phase as they became thicker than ~27 nm. When the films were ~47nm-thick, clear diffraction peaks that could be assigned to the monoclinic phase emerged, which suggests that the films were crystallized well to the monoclinic phase even at their as-deposited state under such ALD condition. Figure 3 (b) shows, from bottom to top, the GAXRD patterns of the as-deposited 45nm-thick HfO_2 films grown under these four different deposition conditions: 280°C O_3; 280°C H_2O; 200°C O_3; and 200°C H_2O. The HfO_2 films grown at the T_s of 280°C crystallized to the monoclinic phase for both oxygen sources, and the HfO_2 film grown under the condition of 200°C H_2O showed very weak crystallization.

Journal of Materials Chemistry C Accepted Manuscript

However, the HfO_2 film grown under the condition of 200°C O_3 showed an almost complete amorphous state despite such thickness. However, the evolution of the crystalline phases upon the PDA of the as-deposited film differed significantly according to the ALD conditions, as shown in Figure 4.

Figures 4 (a)-(d) show the variations in the GAXRD patterns of the four different HfO_2 samples grown under conditions identical to those in Figure 2, which thicknesses were 6 nm, with the increasing PDA temperature (T_{PDA}) of 450°C to 600°C. All the as-deposited samples were amorphous. While the HfO_2 films grown under the conditions of 280°C O_3 and 200°C H_2O were crystallized to the monoclinic phase after the PDA at > 550°C, the HfO_2 films grown under the conditions of 200°C O_3 and 280°C H_2O retained their amorphous structures up to 550°C and crystallized to the mostly tetragonal phase at the T_{PDA} of 600°C. The crystallizations to the monoclinic phase of the films grown under the conditions of 280°C O_3 and 200°C H_2O were normal, as the monoclinic phase is a thermodynamically stable phase. However, the evolution of the HfO_2 phase to the tetragonal phase in the case of the two other conditions had a somewhat unexpected result. As mentioned in the Introduction section, the crystallization of HfO_2 to the tetragonal phase is mainly driven by the grain size effect, and the results shown in Figure 4 (c) could be understood from the viewpoint of the adverse interference effect of carbon impurity with the crystallization and grain growth of the amorphous HfO_2 on the PDA. This is in good agreement with the report of Cho et al. [39], where the ALD of HfO_2 was performed at a T_s of 280°C, with the oxygen source of molecular O_2, the oxidation potential of which was far lower than that of O_3, so that the film had a similar level of carbon impurity concentration (~10%) despite its high T_s. However, the density and AES data shown in Figures 1 (b) and 2 (b) revealed that the HfO_2 films grown under the condition of 280°C H_2O had a low density and a low carbon impurity concentration. This clearly revealed that not only the carbon impurity but also the low density of the as-deposited film induced the crystallization to the tetragonal phase. The low density of the as-deposited film interfered adversely with the grain growth in the PDA and resulted in the tetragonal phase, which was confirmed by the AFM and TEM data that will be shown later. Such trend could be further confirmed by the harsher PDA condition and the thicker thickness. Figure 5

Journal of Materials Chemistry C Accepted Manuscript

shows the GAXRD spectra of the 45nm-thick HfO_2 films grown under the four different conditions after the PDA at 1000°C. The crystalline quality generally increased so that the diffraction peaks became clearer. The HfO_2 films that were grown under the conditions of 280°C O_3 and 200°C H_2O were further crystallized to the monoclinic phase. Interestingly, the HfO_2 film grown under the condition of 280°C H_2O, which was predominantly tetragonal after the PDA at 600°C [Figure 4 (b)], is now predominantly monoclinic. However, the film grown under the condition of 200°C O_3 still has a non-negligible peak intensity that corresponds to the tetragonal phase, although monoclinic phase peaks appeared after this PDA. This suggests that the carbon impurity really interfered with the grain growth and crystallization of the HfO_2 film to the monoclinic phase even at the T_{PDA} of 1000°C.

The correlation between the ALD conditions and the microstructure of the 45nm-thick film after the PDA at 1000°C was further examined via extensive HRTEM analysis. Figure 6 (a)-(d) show the representative HRTEM images of the 45nm-thick HfO_2 films grown under these four different deposition conditions: 280°C O_3; 280°C H_2O; 200°C O_3; and 200°C H_2O after the PDA at 1000°C. For each sample, more than 10 HRTEM images were taken, and at least 20 grain images were analyzed using the fast-Fourier transformation technique to identify their phases. The phase analysis results and the grain size distribution in this TEM study are summarized in Figure 7 and Table I, respectively. While the GAXRD results indicated the phase distribution qualitatively, this TEM analysis showed quantitative distributions of the monoclinic and tetragonal phases in each sample. Interestingly enough, the 200°C H_2O condition resulted in the most dominantly monoclinic phase, and the 200°C O_3 condition resulted in ~30% of the tetragonal phase even after the PDA at 1000°C. The 280°C H_2O condition also showed a high portion (~26%) of the tetragonal phase, which could be understood from its initially low density and low carbon impurity concentration. The 280°C O_3 condition, which was not expected to induce any tetragonal phase due to its high density and low carbon concentration, showed ~15% of the tetragonal phase, which could be ascribed to the presence of Si impurity [48]. The grain size distribution was consistent with the phase distribution. As expected, the 200°C O_3 condition produced the smallest average grain diameter (28.6±8.02 nm), which corresponds well to the highest portion of the tetragonal phase in this sample. The 200°C H_2O condition produced the largest grain

Journal of Materials Chemistry C Accepted Manuscript

diameter (47.7±19.3 nm), which means that this sample has the lowest driving force for the formation of the tetragonal phase. The two other conditions resulted in an intermediate grain diameter, so the intermediate phase distribution in this case could be understood well from the grain size effect.

The crystallization behavior of the HfO_2 films grown under the four different conditions was further examined as a function of the film thickness for different T_{PDA}'s by measuring the RMS roughness of the films using AFM. Although the RMS roughness does not provide direct evidence of the detailed evolution of crystallographic phases in oxide thin films, the increase in such value could be generally ascribed to the accompaniment of the grain formation by crystallization. SEM images can supplement the AFM data. Figures 8 (a)-(d) show the SEM (left panel) and AFM topographic (right panel) images of the 45nm-thick films annealed at 1000°C and deposited under the four different conditions. The morphological images in Figures 8 (a) and (b) allowed estimation of the grain sizes in the two cases, which were 39.5±0.8 nm and 31.6±0.8 nm, respectively, which coincide very well with the data shown in the first and second rows of Table I that were estimated from the TEM. However, the much smoother surface morphologies in Figure 8 (c) and (d) did not allow statistically meaningful grain size estimation.

Figures 9 (a) and (b) show the variations in the RMS roughness measured via AFM of the HfO_2 films deposited under the four different ALD conditions, at the as-deposited state, and after the PDA at 600°C and 1000°C, respectively, as a function of the film thickness. For the cases of 280°C O_3, 280°C H_2O, and 200°C H_2O, the RMS roughness generally increased with the increasing film thickness for all three process conditions, which suggests the increased crystallization with the increasing film thickness. This is coincides well with the GAXRD results shown in Figures 3 and 5. However, the HfO_2 film grown under the condition of 200°C, O3 maintained a very low RMS roughness value irrespective of the thickness in all the PDA conditions. The RMS roughness of the as-deposited film remained at a very low value (~0.2 nm) up to the thickness of 45 nm, which corroborates the complete amorphous structure of this sample. Even after the PDA at 1000°C, the increase in the RMS roughness was very low, which is a remarkable finding considering the obvious crystallization of this sample after the PDA.

Journal of Materials Chemistry C Accepted Manuscript

Next, the chemical binding states of the films grown under the four different conditions were examined via XPS, and the results are correlated with the electrical characteristics. For the XPS examination, no PDA was performed, and the samples for the electrical characterization were annealed under the forming gas condition (see the Experiment section). For the XPS, the SiO_2 film that was thermally grown on Si was also analyzed for reference. In Figures 10 (a) and (b), the C 1s and O 1s spectra of the four ALD HfO_2 films and the SiO_2 samples are shown. All the samples showed clear C 1s peaks, of which C-C BE was set at 284.5 eV. The SiO_2 sample showed the lowest C 1s peak intensity, and the HfO_2 samples showed generally high intensities, which suggest the higher adsorption of adventitious carbon from the atmosphere. In addition, the HfO_2 samples showed non-negligible intensities near the BE of 288.5 eV, which coincides with the hydrocarbon peak that was not observed in the SiO_2 sample. This means that the HfO_2 films contained hydrocarbon impurities that were most probably induced by the incomplete ALD reactions. Such non-ideal aspect of ALD cannot be completely eliminated even for the most favorable ALD conditions (280°C O_3 and 200°C H_2O). The O 1s spectra of the HfO_2 samples showed relatively broad peaks that could be deconvoluted into three components that corresponded to the oxygen ions in the HfO_2 (BE ~530 eV), Hf silicate (BE ~531.5 eV), and SiO_2 (BE ~532.5 eV), whereas that of SiO_2 was composed of only oxygen in the SiO_2. The inclusion of the Hf silicate and SiO_2 components in the HfO_2 films was due to the chemical interaction between the HfO_2 films (or the atmosphere during ALD) and the Si substrate, which could be understood more clearly from the variations in the Si 2p XPS spectra shown in Figures 10 (c) and (d). In the Si 2p spectra, the signal from the Si substrate (BE ~98-98.5 eV) could be clearly observed due to the thinness of the films (~6 nm). Unlike the BE of SiO_2 (~103 eV), the BEs of the oxide peaks from the HfO_2 films shifted into the lower BE direction, which suggests that the ILs were mostly Si sub-oxides or the Hf silicate. The oxide Si 2p peaks from the HfO_2 films deposited under the different ALD conditions were deconvoluted, assuming that there were Si^{4+}, Si^{3+}, Si^{2+}, and Si^{1+} components. The BE of the Si 2p spectra from the Hf silicate is similar to that of Si^{3+} and Si^{2+} [49], so they are not exclusively included in this deconvolution process. Among the four different ALD conditions, the conditions that involved O_3 resulted in the obviously intense peaks,

Journal of Materials Chemistry C Accepted Manuscript

which suggest that the Si substrate was oxidized by the strong oxidation potential of O_3 at the T_s of 280°C and 200°C. In contrast, the conditions that involved H_2O induced a much lower intensity of the oxide Si 2p peak, which reflects the lower oxidation potential of H_2O compared with O_3. The lower T_s also induced the lower oxide peak intensity for both oxygen sources. These observations are well-correlated with the electrical properties, as shown in Figure 11. Figures 10 (e) and (f) show the N 1s XPS peak and valence band (VB) spectra. The N1s peaks had certainly non-negligible intensities compared to the HfO_2 samples, the intensities of which were independent of the ALD conditions. Of course, the SiO_2 film did not show any N 1s peak intensity. This revealed that a non-ideal component of ALD was involved, wherein fragments of the ligands remained and the Hf-N bonding of the Hf-precursor molecules was not completely replaced with the Hf-O bonding in the film. The VB spectra of all the HfO_2 samples are also very similar. Their comparison with the VB of Si provides information on the VB offset between the Si and HfO_2, which is commonly 1.90-1.96 eV. This value is consistent with the theoretical estimations [50-51], but previous reports of experimental results are too extensive, and, thus, were focused on a relative comparison. There are in-gap states that could be ascribed to the presence of impurities, such as C, N, and Si, and only a slight difference in the leakage current - capacitance equivalent thickness (J_g-CET) plots from the different samples for thinner films (< 6 nm), as shown in Figure 12, and such characteristics could be understood from the negligible difference in the VB offset and in-gap states. However, the bulk dielectric properties, represented by the k-values of the different HfO_2 layers, and the thickness of IL could be well- correlated to the XPS signals.

Figure 11 shows the variations in the CET as functions of the physical oxide thickness (POT) of the HfO_2 films grown under the four different ALD conditions, wherein the POT was limited to ~8 nm in (a) and increased to up to ~18nm in (b). The inverse of the slope of the best-linear-fitted graphs of the CET-POT plot indicated the k value of the HfO_2 films, which were free from the influence of any IL, and the y-axis intercept corresponded to the CET of IL, which includes any possible contribution from the interface with the metal electrode [30]. The CET-POT plots showed a change in their slope at POT ~8 nm, except for the 280°C O_3 condition, so the k-values are not constant throughout the entire

Journal of Materials Chemistry C Accepted Manuscript

thickness range. The estimated k-values are summarized in Table II. In the thin thickness range, all the films were mostly amorphous, so the k-values could be mostly determined by the density of the films. However, the highest k-value of ~12.7 from the 280°C O_3 case was still much lower than that of other reports from the amorphous HfO_2 (~15-17 [30, 32-33, and 35-37]). The k-values of the HfO_2 films from the other conditions were even lower (~10.7), which suggests that the thin as-deposited films generally have a low density, which coincides with the density estimation shown in Figure 1 (b). When the films became thicker, some of them started to include crystalline grains even at the as-deposited state, which could have influenced their k-values. The k-values estimated in the POT range of ~9-18 nm were ~17, 26, 22, and 30 for the ALD conditions of 280°C O_3, 280°C H_2O, 200°C O_3, and 200 ^{o}C H_2O, respectively. The lowest k-value of 17 for the condition of 280°C O_3 suggests that the film maintained its amorphous structure with a slightly increased density, which could be ascribed to the self-annealing effect at the ALD temperature for growing the thicker film. The highest k- value of 30 for the condition of 200°C H_2O suggests that the film came to have tetragonal grains, although they could not be clearly identified from GAXRD perhaps due to the still too small grain size of up to 18 nm of POT. The two conditions also showed higher k-values than in the thinner film cases, which suggests that there was an increase in the crystallinity that contained the non-negligible concentration of the tetragonal phase, which could not be detected via GAXRD.

The y-axis intercept in Figure 11 (a) clearly shows that the conditions that involved O_3 induced a thicker IL, the CET of which was ~0.8 nm, whereas the two other conditions that involved H_2O induced an IL CET of as small as ~0.2 nm. This coincided well with the higher and lower oxide peak intensities in the Si 2p XPS spectra in the former and latter cases, respectively, which suggests the higher interfacial oxidation of Si in the former case.

Figure 12 summarizes the J_g-CET plots of the HfO_2 films grown under the four ALD conditions. As the HfO_2 films grown under the different conditions had different flat-band voltages (V_{fb}), J_g was estimated at the gate voltage of V_{fb}-1 V. Within the smallest CET range of ~1.5-2.0 nm, the HfO_2 films grown under the condition of 200°C H_2O showed the lowest J_g level, which could be ascribed to the fluent ALD mechanism in such condition that resulted in the high density and the low impurity

Journal of Materials Chemistry C Accepted Manuscript

concentration. The J_g-CET performance was comparable to the state-of-the-art levels of the TEMAH-H_2O and TEMAH-O_3 ALD processes performed at 345°C, as reported by the IMEC group [18], even though in this study, a much lower T_s (200°C H_2O) was adopted. However, as the CET exceeded ~3 nm, the J_g level of the samples deposited under the conditions that involved H_2O became higher than that of the samples deposited under the conditions that involved O_3 by ~1-2 orders of magnitude. Such result requires further investigation for accurate understanding. Hydrogen content could be different in the various types of the films in this work, which could have quite large influence on the electrical properties. However, quantitative determination of the hydrogen content is generally difficult, so it was not attempted. Meanwhile, the hydrogen might be present in the form of hydrocarbons, so correlating the electrical properties with the carbon concentration could be an indirect indication of correlation between the property and the hydrogen content.

IV. Conclusion

The effects of O_3 and H_2O as oxygen sources on the ALD of HfO_2 films grown at substrate temperatures of 160-360°C were examined in terms of their growth characteristics and structural evolution upon the thickness increase and post-deposition annealing. While the ALD process that involved H_2O was achieved well at a temperature as low as 160°C, the ALD in which O_3 was used required substrate temperatures of 240-280°C to induce a fluent ALD reaction. This could be ascribed to the proton-induced ligand exchange reaction in the case of the ALD with H_2O, whereas the O-radical mediated ALD reaction appeared to require supply of thermal energy to overcome its rather high activation energy. According to these different ALD mechanisms, the HfO_2 films grown at 200°C and 280°C for the ALD that involved H_2O and O_3, respectively, showed the highest density. The HfO_2 films with a low density or (and) a high carbon-impurity concentration crystallized to the tetragonal phase after the PDA at 600°C, whereas the thin film with both a low density and high carbon impurity retained the highest portion of the tetragonal phase (~30%) even after the PDA at 1000°C. While the majority phase of the crystalline materials was monoclinic phase by the increasing thickness or PDA temperature, all the HfO_2 films contained a non-negligible concentration of the tetragonal phase,

Journal of Materials Chemistry C Accepted Manuscript

which was found from the extensive and detailed HRTEM study. This could be related to the presence of the film surface with a lower energy for the phases other than the monoclinic phase. The density of the thin as-deposited films (< 8 nm) was important in the determination of the bulk dielectric constant, and the bulk dielectric constants of the thicker films (8-18 nm) were contributed by the (partial) crystalline phase and the density. The best electrical performance was achieved in the HfO_2 film grown at 200°C with H_2O due to the minimum-involvement of the interfacial oxide layer and the high bulk density of the film.

Acknowledgment

The authors acknowledge the support of the Converging Research Center Program of the National Research Foundation of Korea (NRF), which is funded by the Ministry of Education, Science, and Technology (2013K000158).

Journal of Materials Chemistry C Accepted Manuscript

References

1. G. D. Wilk, R. M. Wallace, J. M. Anthony, *J. Appl. Phys.*, 2001, **89**, 5243.
2. International Technology Roadmap for Semiconductor (2011, 2012 update)
3. http://www.intel.com/content/www/us/en/architecture-and-technology/microarchitecture/microarchitecture-overview-general.html
4. A. Delibie, F. Bellenger, M. Houssa, T. Conard, S. Van Elshocht, M. Caymax, M. Heyns, and M. Meuris, *Appl. Phys. Lett.*, 2007, **91**, 082904.
5. F. Bellenger, M. Houssa, A. Delibie, V. Afanasiev, T. Conard, M. Caymax, M. Meuris, K. De Meyer, and M. M. Heyns, *J. Electrochem. Soc.*, 2008, **155**, G33.
6. A. Delibie, A. Alian, F. Bellenger, M. Caymax, T. Conard, A. Franquet, S. Sioncke, S. Van Elshocht, M. M. Heyns, and M. Meuris, *J. Electrochem. Soc.*, 2009, **156** (10) G163.
7. S. Spiga, C. Wiemer, G. Tallarida, G. Scarel, S. Ferrari, G. Seguini, and M. Fanciulli, *Appl. Phys. Lett.*, 2005, **87**, 112904.
8. Y.-C. Byun, C. Mahata, C.-H. An, J. Oh, R. Choi, and H. Kim, *J. Phys. D: Appl. Phys.*, 2012, **45**, 435305.
9. L. Lamagna, G. Scarel, M. Fanciullib, and G. Pavia, *J. Vac. Sci. Technol. A*, 2009, **27** (3), 443.
10. G. Mavrou, S. Galata, P. Tsipas, A. Sotiropoulos, Y. Panayiotatos, A. Dimoulas, E. K. Evangelou, J. W. Seo, and Ch. Dieker, *J. Appl. Phys.*, 2008, **103**, 014506.
11. L. Lamagna, C. Wiemer, M. Perego, S. N. Volkos, S. Baldovino, D. Tsoutsou, S. Schamm-Chardon, P. E. Coulon, and M. Fanciulli, *J. Appl. Phys.*, 2010, **108**, 084108.
12. Y. Liu, M. Xu, J. Heo, P. D. Ye, and R. G. Gordon, *Appl. Phys. Lett.*, 2010, **97**, 162910.
13. D. H. Triyoso, R. I. Hegde, B. E. White Jr., and P. J. Tobin, *J. Appl. Phys.*, 2005, **97**, 124107.
14. M. Ritala, M. Leskelä, L. Niinistö, T. Prohaska, G. Friedbacher, M. Grasserbauer, *Thin Solid Films*, 1994, **250**, p. 72.
15. J. Aarik, A. Aidla, A.-A. Kiisler, T. Uustare, V. Sammelselg, *Thin Solid Films*, 1999, **340**, p. 110.
16. M. Cho, H. B. Park, J. Park, S. W. Lee, C. S. Hwang, J. Jeong, H. S. Kang, and Y. W. Kim, *J. Electrochem. Soc.*, 2005, **152** (5), F49.

Journal of Materials Chemistry C Accepted Manuscript

17. X. Liu, S. Ramanathan, A. Longdergan, A. Srivastava, E. Lee, T. E. Seidel, J. T. Barton, D. Pang, and R. G. Gordon, *J. Electrochem. Soc.*, 2005, **152** (3), G213.
18. J. Swerts, N. Peys, L. Nyns, A. Delabie, A. Franquet, J. W. Maes, S. V. Elshocht, and S. D. Gendt, *J. Electrochem. Soc.*, 2010, **157** (1), G26.
19. T. J. Park, J. H. Kim, M. H. Seo, J. H. Jang, and C. S. Hwang, *Appl. Phys. Lett.*, 2007, **90**, 152906.
20. C. S. Hwang (Ed.) Atomic Layer Deposition for Semiconductors, Chap. 7. Springer, 2014. ISBN 978-1-4614-8054-9
21. A. C. Jones, H. C. Aspinall, P. R. Chalker, R. J. Potter, T. D. Manning, Y. F. Loo, R. O'Kane, J. M. Gaskell, L. M. Smith, *Chem. Vap. Deposition*, 2006, **12**, 83.
22. K. Kukli, M. Ritala, M. Leskelä, T. Sajavaara, J. Keinonen, *Chem. Vap. Deposition*, 2002, **8**, 199.
23. K. Kukli, T. Pilvi, M. Ritala, J. Lu, , M. Leskelä, *Thin Solid Films*, 2005, **491**, 328.
24. J. Niinistö, M. Mäntymäki, K. Kukli, L. Costelle, E. Puukilainen, M. Ritala, and M. Leskelä, *J. Crystal Growth*, 2010, **312**, 245.
25. J. Niinistö, M. Putkonen, L. Niinistö, F. Song, P. Williams, P. N. Heys, and R. Odedra, *Chem. Mat.*, 2007, **19**, 3319.
26. J. Swerts, N. Peys, L.a Nyns, A. Delabie, A. Franquet, J. W. Maes, S. V. Elshocht, and S. De Gendt, *J. Electrochem. Soc.*, 2010, 157 (1), G26.
27. S. Kamiyama, T. Miura, and Y. Nara, *Electrochem. Solid-state Lett.*, 2006, **9** (9) G285.
28. C. Choi, C.-Y. Kang, S. J. Rhee, M. S. Akbar, S. A. Krishnan, M. Zhang, H.-S. Kim, T. Lee, I. Ok, F. Zhu, and J. C. Lee, *IEDM Tech. Dig.*, 2005, Vol. **26**, No. 7, 454.
29. L. Wu, H.Y. Yu, X. Li, K.L. Pey, K.Y. Hsu, H.J. Tao, Y.S. Chiu, C.T. Lin, J.H. Xu, H.J. Wan, International Symposium on VLSI Technology Systems and Applications (VLSI-TSA), 2010, 90.
30. H. K. Kim, S. Y. Lee, I.-H. Yu, T. J. Park, R. Choi, and C. S. Hwang, *IEEE Electron Device Lett.*, 2012, pp. 955.
31. J. H. Kim, T. J. Park, S. K. Kim, D.-Y. Cho, H.-S. Jung, S. Y. Lee, and C. S. Hwang, Accepted, *Appl. Surf. Sci.*
32. X. Zhao and D. Vanderbilt, *Phys. Rev. B*, 2002, **65**, 233106.

Journal of Materials Chemistry C Accepted Manuscript

33. T.-J. Chen and C.-L. Kuo, *J. Appl. Phys.*, 2011, **110**, 064105.

34. J. Tang, F. Zhang, P. Zoogman, Jason Fabbri, S.-W. Chan, Y. Zhu, L. E. Brus, and M. L. Steigerwald, *Adv. Func. Mater.*, 2005, **15**, 1595-1602.

35. D. Fisher and A. Kersch, *Appl. Phys. Lett.*, 2008, **92**, 012908.

36. H.-S. Jung, H. K. Kim, I.-H. Yu, S. Y. Lee, J. Lee, J. Park, J. H. Jang, S.-H. Jeon, Y. J. Chung, N.-I. Lee, T. J. Park, J.-H. Choi, and C. S. Hwang, *J. Electrochem. Soc.*, 2012, **159**, G33.

37. H.-S. Jung, S. H. Jeon, H. K. Kim, I.-H. Yu, S. Y. Lee, J. Lee, Y. J. Chung, D.-Y. Cho, N.-I. Lee, T. J. Park, J.-H. Choi, S. Han, and C. S. Hwang, *ECS J. Sol. Sta. Sci. and Technol.*, 2012, **1** (2), N33.

38. J. Schaeffer, N. V. Edwards, R. Liu, D. Roan, B. Hradsky, R. Gregory, J. Kulik, E. Duda, L. Contreras, J. Christiansen, S. Zollner, P. Tobin, B.-Y. Nguyen, R. Nieh, M. Ramon, R. Rao, R.Hedge, R. Rai, J. Baker, and S. Voight, *J. Electrochem. Soc.*, 2003, **150**, F67.

39. D.-Y. Cho, H. S. Jung, I.-H. Yu, J. H. Yoon, H. K. Kim, S. Y. Lee, S. H. Jeon, S. Han, J. H. Kim, T. J. Park, B.-G. Park, and C. S. Hwang, *Chem. Mater.*, 2012, **24**, 3534.

40. J.I. Beltrán, M.C. Muñoz, J. Hafner, *New J. Phys.*, 2008, **10**, 063031.

41. O. Ohtaka, H. Fukui, T. Kunisada, and T. Fujisawa, *J. Am. Ceram. Soc.*, 2001, **84**, 1369-73.

42. T.S. Böscke, P.Y. Hung, P.D. Kirsch, M.A. Quevedo-Lopez, R. Ramírez-Bon, *Appl. Phys. Lett.*, 2009, **95**, 052904.

43. J. Wang, *J. Mater. Sci.*, 1992, **27**, 5397-5430.

44. M. Shandalov, P.C. McIntyre, *J. Appl. Phys.*, 2009, 106, 084322.

45. J. R. Hauser, CVC ©2000 NCSU software, version 5.0, Dept. Electr. Comput. Eng. North Carolina State University, Raleigh, NC.

46. M. Shirazi, and S. D. Elliott, *Chem. Mater.*, 2013, **25**, 878-889.

47. J. Niinistö, M. Putkonen, L. Niinistö, K. Arstila, T. Sajavaara, J. Lu, K. Kukli, M. Ritala, and M. Leskelä, *J. Electrochem. Soc.*, 2006, **153** (3), F39.

48. H. K. Kim, H.-S. Jung, J. H. Jang, J. Park, T. J. Park, S.-H. Lee, and C. S. Hwang, *J. Appl. Phys.*, 2011, **110**, 114107.

49. J. Wang, B. Mao, M. G. White, C. Burda, and J. L. Gole, *RSC Adv.*, 2012, **2**, 10209.

Journal of Materials Chemistry C Accepted Manuscript

50. E. Bersch, S. Rangan, and R. A. Bartynski, E. Garfunkel, E. Vescovo, *Phys. Rev. B*, 2008, **78**, 085114.

51. W.-C. Huang, H.-W. Ting, K.-M. Hung, J.-H. Yin, K.-H. Chou and H.-C. Chang, *Multimedia Technology (ICMT), International Conference*, 2011.

Journal of Materials Chemistry C Accepted Manuscript

List of Figures

1. Variations in the (a) growth rate and (b) film density, measured via the XRR of the HfO_2 films with O_3 and H_2O oxidants as a function of T_s (160-360°C)
2. AES depth profile of the HfO_2 films under these four deposition conditions: (a) 280°C O_3, (b) 280°C H_2O, (c) 200°C O_3, and (d) 200°C H_2O
3. GAXRD spectra of the (a) as-deposited HfO_2 films that thickened when the films were grown at a T_s of 280°C using O_3, and (b) as-deposited 45nm-thick HfO_2 films grown under these four different deposition conditions: 280°C O_3, 280°C H_2O, 200°C O_3, and 200°C H_2O, from bottom to top
4. Variations in the GAXRD patterns of the four different HfO_2 samples: (a) 280°C O_3, (b) 280°C H_2O, (c) 200°C O_3, and (d) 200°C H_2O, the thickness of which was 6 nm, with the increase in the PDA temperature (T_{PDA}) from 450°C to 600°C
5. GAXRD spectra of the 45nm-thick HfO_2 films grown under the four different conditions after the PDA at 1000°C
6. HRTEM images of the 45nm-thick HfO_2 films grown under these four different deposition conditions: (a) 280°C O_3, (b) 280°C H_2O, (c) 200°C O_3, and (d) 200°C H_2O after the PDA at 1000°C
7. Phase ratios of the HfO_2 films using the O_3 and H_2O grown at (a) 280°C and (b) 200°C, from the TEM analysis, via the statistical analysis of the HR images
8. SEM (left panel) and AFM topographic (right panel) images of the 45nm-thick films annealed at 1000°C and deposited under these four different conditions: (a) 280°C O_3, (b) 280°C H_2O, (c) 200°C O_3, and (d) 200°C H_2O
9. Variations in the RMS roughness, measured via AFM of the HfO_2 films deposited using (a) O_3 and (b) H_2O grown on 280°C (closed data) and 200°C (open data) at the as-deposited state, and after the PDA at 600 and 1000°C, respectively, as functions of the film thickness
10. XPS spectra of the (a) C 1s, (b) O 1s, (c) Si 2p, and (d) Si 2p that were deconvoluted assuming the Si^{4+}, Si^{3+}, Si^{2+}, and Si^{1+} components, (e) the N 1s, and (f) the valence band for the four different

Journal of Materials Chemistry C Accepted Manuscript

deposition conditions of HfO_2 (280^oC O_3, 280^oC H_2O, 200^oC O_3, and 200^oC H_2O) and the thermally grown SiO_2 as references

11. CET variations as functions of the physical oxide thickness (POT) for the HfO_2 films grown under the four different ALD conditions, wherein the POT was limited to ~8 nm in (a) and increased to up to ~18 nm in (b)
12. J_g-CET plots of the HfO_2 films grown under the four ALD conditions

Journal of Materials Chemistry C Accepted Manuscript

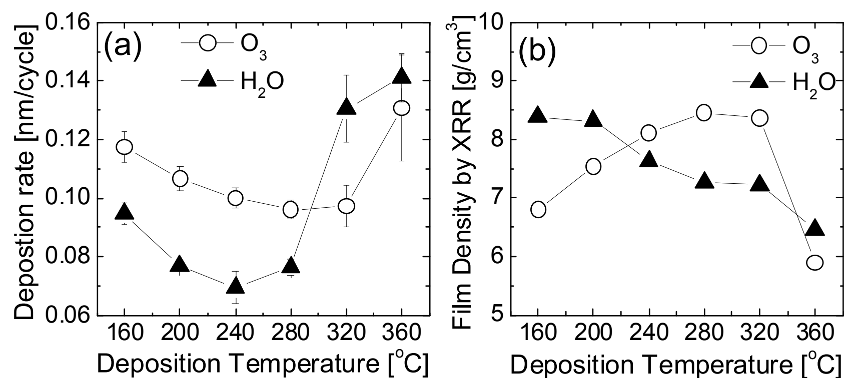

Fig. 1 Variations in the (a) growth rate and (b) film density, measured via the XRR of the HfO_2 films with O_3 and H_2O oxidants as a function of T_s (160-360°C)

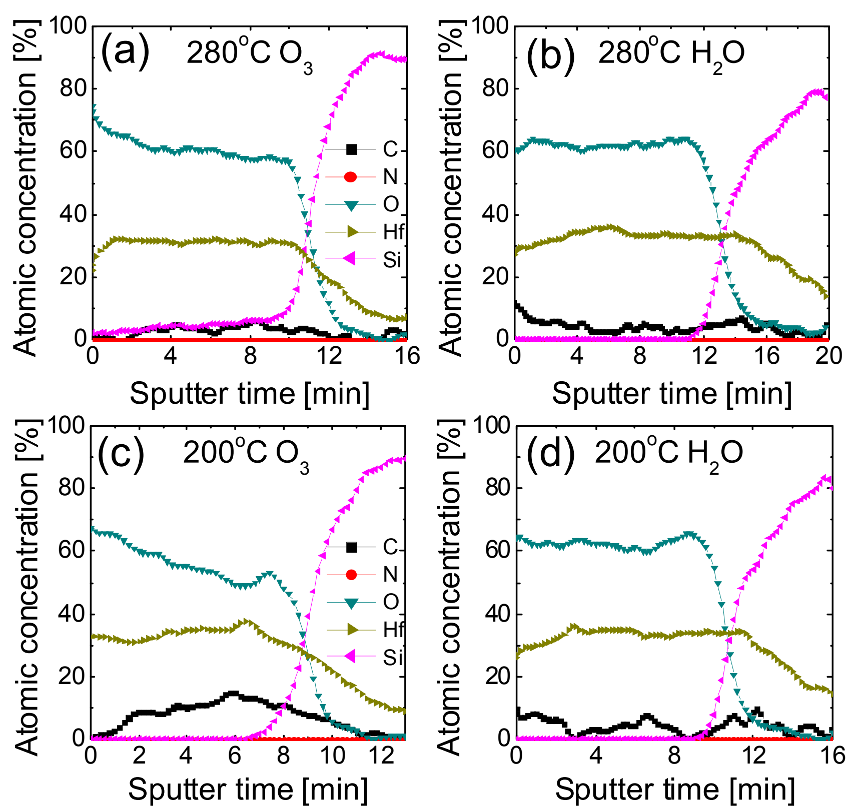

Fig. 2 AES depth profile of the HfO_2 films under these four deposition conditions: (a) 280°C O_3, (b) 280°C H_2O, (c) 200°C O_3, and (d) 200°C H_2O

Journal of Materials Chemistry C Accepted Manuscript

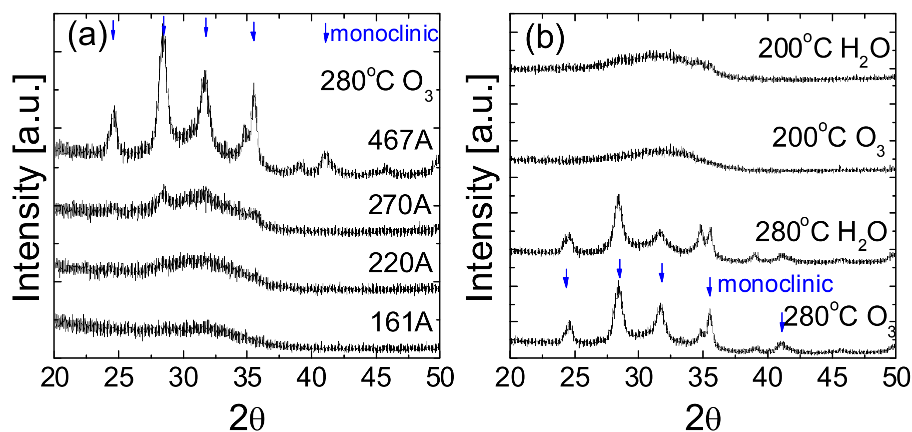

Fig. 3 GAXRD spectra of the (a) as-deposited HfO_2 films that thickened when the films were grown at a T_s of 280°C using O_3, and (b) as-deposited 45nm-thick HfO_2 films grown under these four different deposition conditions: 280°C O_3, 280°C H_2O, 200°C O_3, and 200°C H_2O, from bottom to top

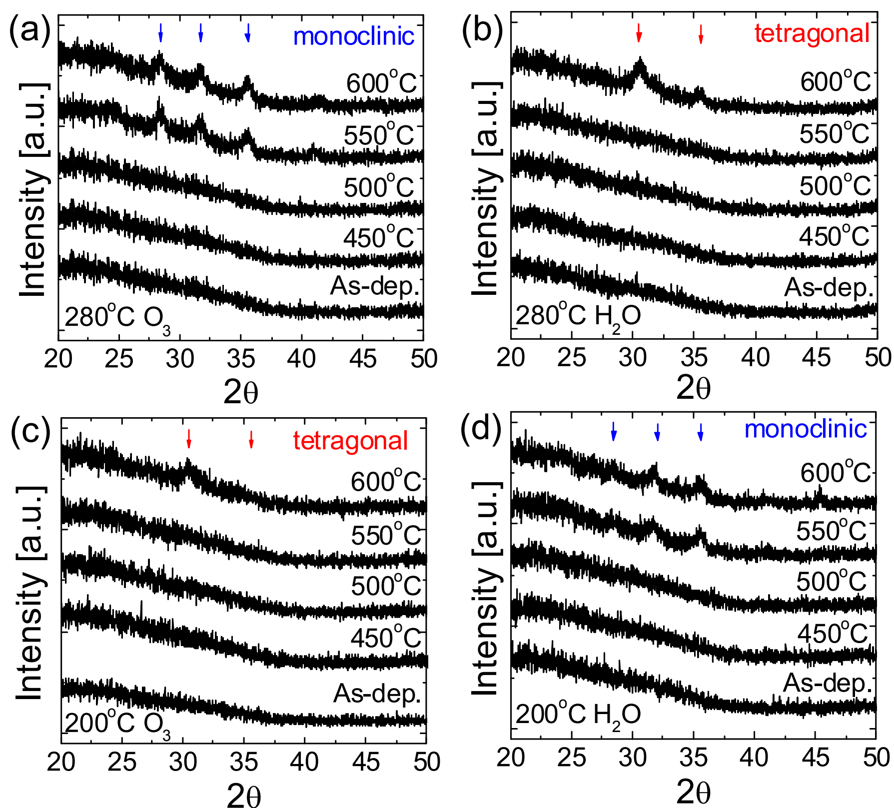

Fig. 4 Variations in the GAXRD patterns of the four different HfO_2 samples: (a) 280°C O_3, (b) 280°C H_2O, (c) 200°C O_3, and (d) 200°C H_2O, the thickness of which was 6 nm, with the increase in the

Journal of Materials Chemistry C Accepted Manuscript

PDA temperature (T_{PDA}) from 450°C to 600°C

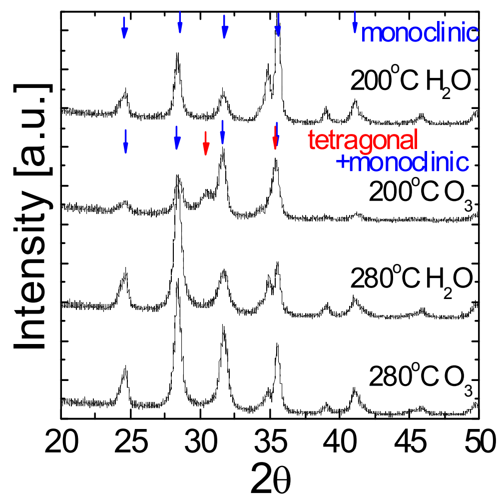

Fig. 5 GAXRD spectra of the 45nm-thick HfO_2 films grown under the four different conditions after the PDA at 1000°C

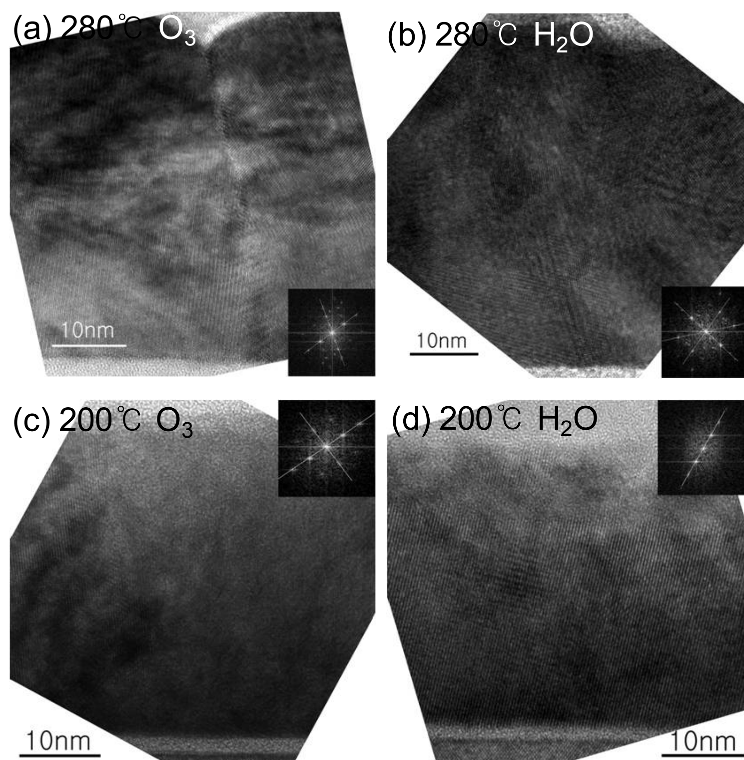

Fig. 6 HRTEM images of the 45nm-thick HfO_2 films grown under these four different deposition conditions: (a) 280°C O_3, (b) 280°C H_2O, (c) 200°C O_3, and (d) 200°C H_2O after the PDA at 1000°C

Journal of Materials Chemistry C Accepted Manuscript

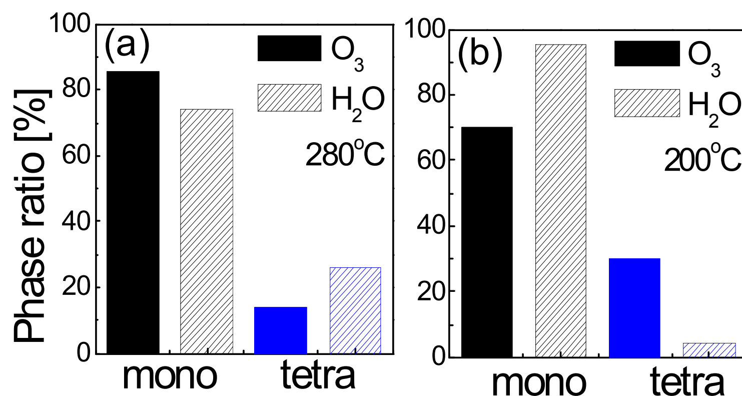

Fig. 7 Phase ratios of the HfO_2 films using the O_3 and H_2O grown at (a) 280°C and (b) 200°C, from the TEM analysis, via the statistical analysis of the HR images

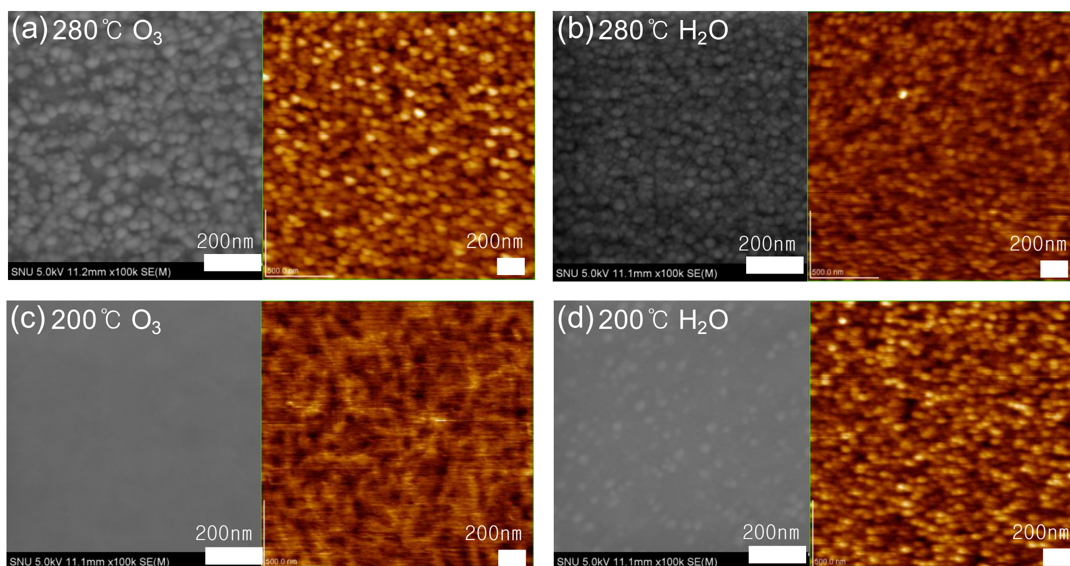

Fig. 8 SEM (left panel) and AFM topographic (right panel) images of the 45nm-thick films annealed at 1000°C and deposited under these four different conditions: (a) 280°C O_3, (b) 280°C H_2O, (c) 200°C O_3, and (d) 200°C H_2O

Journal of Materials Chemistry C Accepted Manuscript

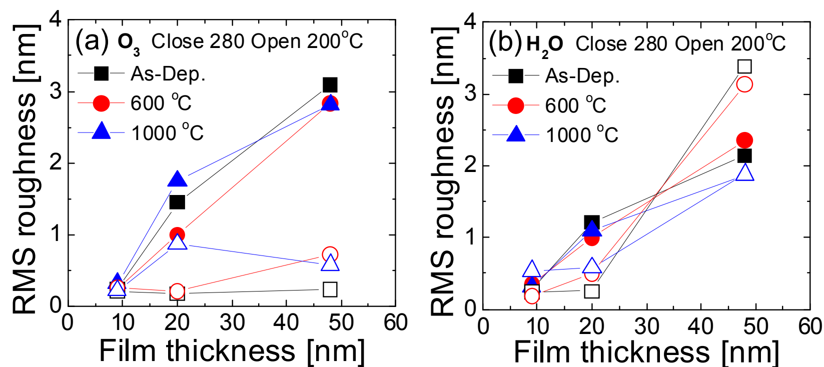

Fig. 9 Variations in the RMS roughness, measured via AFM of the HfO_2 films deposited using (a) O_3 and (b) H_2O grown on 280°C (closed data) and 200°C (open data) at the as-deposited state, and after the PDA at 600 and 1000°C, respectively, as functions of the film thickness

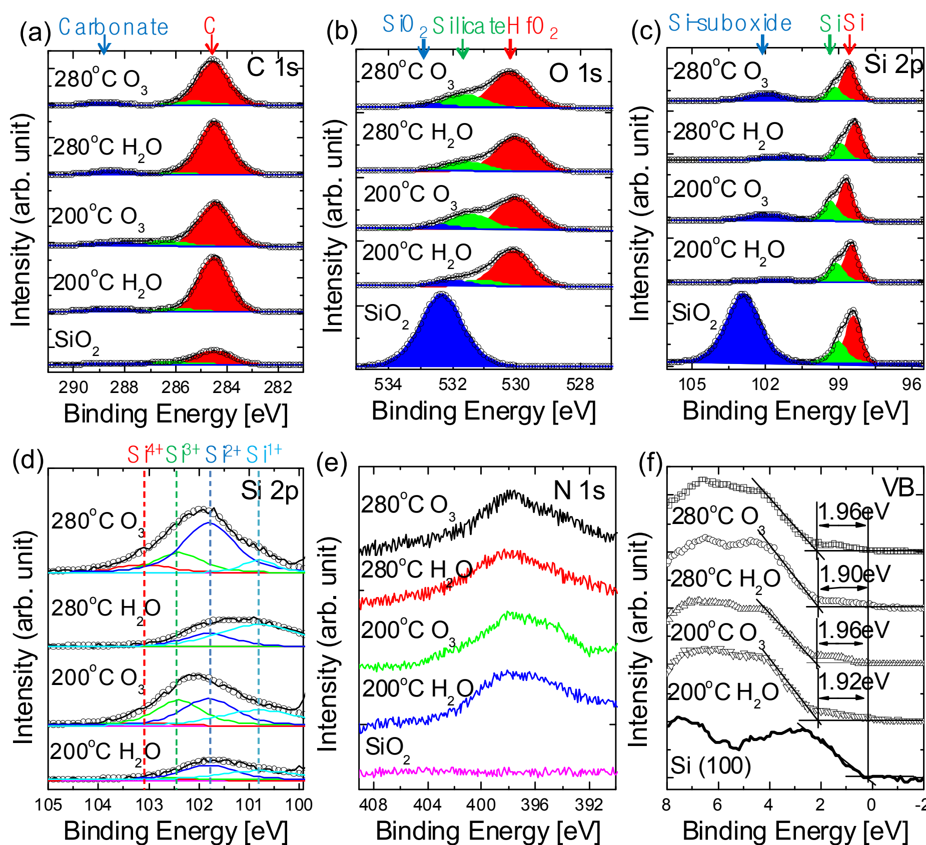

Fig. 10 XPS spectra of the (a) C 1s, (b) O 1s, (c) Si 2p, and (d) Si 2p that were deconvoluted assuming the Si^{4+}, Si^{3+}, Si^{2+}, and Si^{1+} components, (e) the N 1s, and (f) the valence band for the four different deposition conditions of HfO_2 (280°C O_3, 280°C H_2O, 200°C O_3, and 200°C H_2O) and the thermally grown SiO_2 as references

Journal of Materials Chemistry C Accepted Manuscript

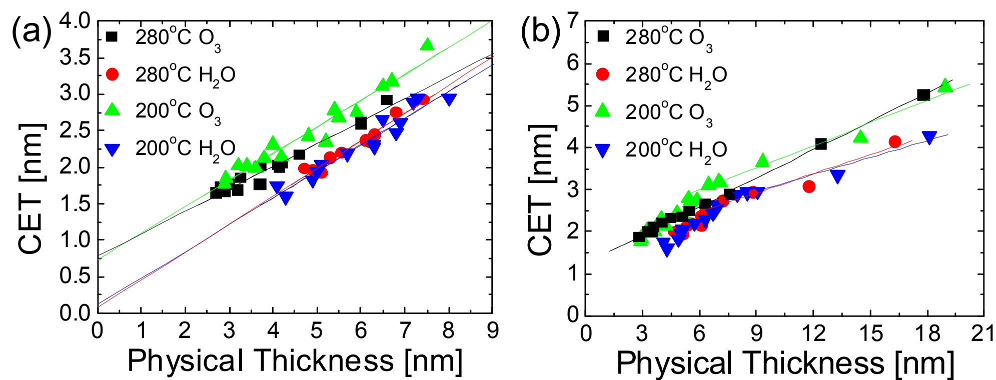

Fig. 11 CET variations as functions of the physical oxide thickness (POT) for the HfO_2 films grown under the four different ALD conditions, wherein the POT was limited to ~8 nm in (a) and increased to up to ~18 nm in (b)

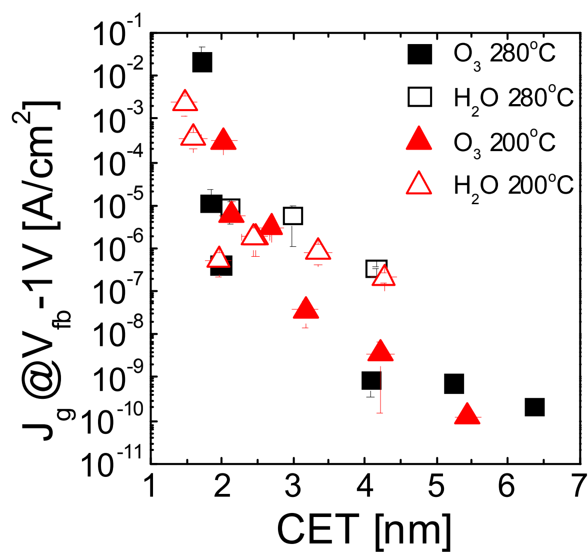

Fig. 12 J_g-CET plots of the HfO_2 films grown under the four ALD conditions

Journal of Materials Chemistry C Accepted Manuscript

Tables

Table I. Grain size distribution from the TEM bright field images via statistical analysis of the HR images

Deposition condition of HfO_2 films	Average grain size [nm]	Standard deviation [nm]
280℃ O_3	37.6	9.66
280℃ H_2O	33.4	6.94
200℃ O_3	28.6	8.02
200℃ H_2O	47.7	19.3

Table II. Dielectric constant k values of the thin (less than 8 nm) and thick thickness ranges of the HfO_2 films grown under the four ALD conditions

Deposition condition of HfO_2 films	Dielectric constant in thin thickness range	Dielectric constant in thick thickness range
280℃ O_3	12.7	17.3
280℃ H_2O	10.2	25.7
200℃ O_3	10.7	22.0
200℃ H_2O	10.7	29.4

Journal of Materials Chemistry C Accepted Manuscript

ToC graphic : Variations in the (a) growth rate and (b) film density, measured via the XRR of the HfO_2 films with O_3 and H_2O oxidants as a function of T_s (160-360°C)

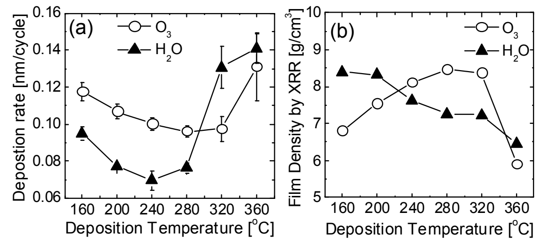

Journal of Materials Chemistry C Accepted Manuscript